



# Comprehensive Study of Morphological Modification of Dual-Layer Hollow Fiber Membrane

Silvana Dwi Nurherdiana<sup>1,2</sup> · Wahyu Prasetyo Utomo<sup>1</sup> · Happy Bunga Naszirahul Sajidah<sup>1,2</sup> · Siti Munira Jamil<sup>2,3</sup> · Mohd Hafiz Dzarfan Othman<sup>2</sup> · Hamzah Fansuri<sup>1</sup>

Received: 22 February 2019 / Accepted: 22 July 2019 / Published online: 31 July 2019  
© King Fahd University of Petroleum & Minerals 2019

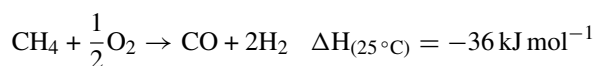
## Abstract

The NiO–YSZ/LSCF–YSZ dual-layer hollow fiber membrane receives increasing attention which is due liable to quick changes in properties during co-extrusion followed by the co-sintering method. The effect of mixed bore liquid of water + ethanol + *n*-methyl-2-pyrrolidone and co-sintering temperature on physical and chemical characteristics of the obtained membrane was systematically explored in this study. Here, the characterization of the membrane was inspected using scanning electron microscope–energy-dispersive X-ray, three-point bending, mercury porosimetry, X-ray diffraction and nitrogen tightness tests as well as the oxygen permeation test. Results indicated that membrane prepared using 100% water as a bore liquid produced a sandwich structure. On the contrary, by employing 40:10:50% of water/ethanol/NMP as a mixed bore liquid and sintering for 8 h at 1300 °C, an open-channel structure in the microstructure gives a good porosity as tested using mercury porosimetry, mechanical properties and nitrogen permeability with no secondary phases. In addition, the co-sintering effect was examined by increasing temperature to 1400 and 1500 °C. However, an impurity phase of LaZr<sub>2</sub>O<sub>7</sub> was formed which is due to the chemical reaction of La and Sr into YSZ structure. Oxygen permeate concentration through the dual-layer membrane was found to be slightly different as compared to the single-layer hollow fiber membrane. The results further suggest that the outer layer should be tighter and thinner to enhance the oxygen ion diffusion.

**Keywords** Hollow fiber membrane · Perovskite membrane · Bore liquid · Pore configuration · NiO–YSZ/LSCF–YSZ

## 1 Introduction

Syngas, mixture of carbon monoxide and hydrogen (CO + H<sub>2</sub>), which is defined as a raw material for petrochemical and energy industry, can be obtained from the reaction between methane and oxygen in a specific ratio via partial oxidation of methane (POM) using a catalyst membrane which involved an exothermic reaction:



The main drawback of the current catalyst is high local heating and leakage (planar form) and low specific area (tubular and single-layer hollow fiber form), which contributes to low methane conversion, syngas selectivity and high carbon deposition [1].

A ceramic hollow fiber membrane of La<sub>x</sub>Sr<sub>1-x</sub>Co<sub>y</sub>Fe<sub>1-y</sub>O<sub>3-δ</sub> (LSCF) was commonly promoted as a catalyst in POM reaction due to its mixed ionic and electronic conductivity behavior due to which oxygen is able to separate from the air through the membrane and sequentially react with methane to produce the desired product [2]. However, carbon deposition was found on the LSCF single-layer membrane, which reduced CO selectivity from 89.4% (15th cycle) to 35% (29th cycle) [3]. To overcome the problems, a dual-layer hollow fiber membrane has been developed. The membrane is composed of NiO catalyst

✉ Hamzah Fansuri  
h.fansuri@chem.its.ac.id

<sup>1</sup> Department of Chemistry, Faculty of Science, Institut Teknologi Sepuluh Nopember, Kampus ITS Sukolilo, Surabaya 60111, Indonesia

<sup>2</sup> Advanced Membrane Technology Research Centre (AMTEC), School of Chemical and Energy Engineering, Universiti Teknologi Malaysia (UTM), 81310 Johor Bahru, Malaysia

<sup>3</sup> Centre for Degree Programme, School of Professional and Continuing Education (UTMSPACE), Universiti Teknologi Malaysia (UTM), 81310 Johor Bahru, Malaysia



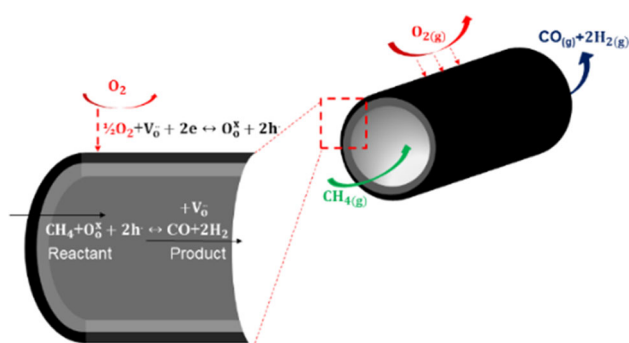


**Fig. 1** Schematic illustration of partial oxidation of methane reaction to syngas over perovskite-based catalyst membrane

which is supported by perovskite which has high catalytic activity and carbon toxicity resistance [4].

Referring to the work by Wu et al. [4] and Mohamed et al. [5], over the past 5 years, a dual-layer NiO–YSZ/LSCF–YSZ membrane was successfully fabricated using co-extrusion method. NiO and YSZ were used as inner layer materials in the dual-layer membranes as electronic and ionic conductors, respectively. The YSZ was also added to the LSCF (outer) layer to prevent oxygen ion blockage in the interface between the two layers as illustrated in Fig. 1. Wu et al. [4] reported that the use of dual-layer membrane produces 95% CO selectivity, which is greater than CO selectivity (89.4%) of a single-layer membrane reported by Dai et al. [3], operated at the same temperature (900 °C) for 30 min. Therefore, the dual-layer hollow fiber membrane has received more attention in producing an impactful simultaneous catalytic performance than single-layer membrane.

According to the previous research, the morphology of the dual-layer hollow fiber membrane plays an important role in obtaining high compatibility between both layers and good membrane performance especially to avoid leakage and local catalytic reactions. Thus, the asymmetric structure which combines finger-like structure and sponge-like structure was the most preferable [6–9]. Yang et al. [10] reported that a membrane, where a dense layer is sandwiched between layers with finger-like pores, has lower oxygen permeability than non-sandwiched structure. The morphology of membrane can be adjusted by controlling factors that affect microstructures such as precursor composition, bore liquid, extrusion rate, air gap and sintering process.

A mixture of water + N-methyl-2-pyrrolidone (NMP) and ethanol + NMP had been used as a bore liquid by Tan et al. [8]. The results showed that water + NMP with a ratio of 1:9 (v/v) and ethanol + NMP of the same ratio produced different oxygen permeation fluxes, i.e., 1.61 and 1.89 mL cm<sup>-2</sup> min<sup>-1</sup>, respectively. Ethanol + NMP produced membranes with higher flux. However, it sacrifices the mechanical strength. The membranes were brittle and easily cracked due to low pore configuration regularity.

The interaction between suspension and bore liquid initiated the finger-like and/or macro-void pores formation before being immersed in the water bath as an external coagulant (EC). Therefore, the mixing of balancing control, i.e., water and NMP in ethanol will provide the best of our membrane fabrication knowledge due to no studies on the previous literature.

In addition to bore liquid, sintering process as the final preparation step in membrane fabrication also affects the thickness and density of the sponge-like pore layer, finger-like pore consistency and the performance on oxygen permeability [2, 11]. The difference in microstructure formation of NiO–YSZ/LSCF–YSZ membrane was examined using sintering temperature at 1100, 1200 and 1300 °C and has been reported. The mechanical strength of the membrane was increased from 18.9 to 32.5 MPa when the membrane was sintered at the highest temperature [5]. However, high sintering temperature may decrease the membrane permeability and change the precursor crystal structure, particularly on perovskite oxides membranes, which reduced oxygen ion migration through the crystal lattice [12, 13].

Concerning the microstructure problems toward pore controlling and sintering effects, herein, we provide the investigation of the water + ethanol + NMP mixture as a bore liquid in La<sub>0.7</sub>Sr<sub>0.3</sub>Co<sub>0.2</sub>Fe<sub>0.8</sub>O<sub>3-δ</sub>-YSZ/NiO–YSZ dual-layer hollow fiber membrane morphology which is fabricated using co-extrusion followed by co-sintering method. In addition, phase evolution and oxygen permeate concentration test of the membrane materials were also examined for the best knowledge of the dual-layer hollow fiber membrane preparation.

## 2 Experimental

### 2.1 Materials

La<sub>0.7</sub>Sr<sub>0.3</sub>Co<sub>0.2</sub>Fe<sub>0.8</sub>O<sub>3-δ</sub> (LSCF 7328) powder was prepared using the solid-state method which had been described in detail by Nurherdiana et al. [14]. Commercially available nickel (II) oxide (NiO 0.47 m<sup>2</sup> g<sup>-1</sup>) and 8 mol% yttria-stabilized zirconia (YSZ 1.7 m<sup>2</sup> g<sup>-1</sup>) were, respectively, used as ionic conductor to facilitate the passage of oxygen ions through the membrane and the thermal barrier coating to attain the difference in thermal expansion coefficient between LSCF and NiO material [15]. Polyether-sulfone (PESf, Radel A300, Ameco Performance, USA) was used as the polymeric binder for membrane formation. Poly(vinylpyrrolidone) (PVP) with Mw = 10,000 Da was used as an additive which initiates a high dope viscosity and reduces the miscibility of the dope solution with non-solvent. NMP (Merck, purity ≥ 99.5%) was used as a solvent due to its characteristics that offer good solubility in the starting

**Table 1** Parameter condition of NiO–YSZ/LSCF–YSZ fabrication

Parameter condition	NiO-YSZ (inner layer)	LSCF-YSZ (outer layer)
Dope composition (wt%)		
LSCF 7328	–	18
YSZ	28	42
NiO	42	–
NMP	22.9	33.9
PESf	7	6
PVP (Mw = 10,000)	0.1	0.1
Extrusion rate (mL min <sup>-1</sup> )	8	6
Outer/inner diameter (mm)	3.0/1.5	
Bore liquid	Water/ethanol/NMP	
Flow rate of bore liquid (mL min <sup>-1</sup> )	8–12	
External coagulant (EC)	Tap water	
Air gap (cm)	10	
Sintering temperature(°C)	1200–1500	
Sintering time (h)	8	
Sintering rate (°C min <sup>-1</sup> )	5–10	

solution [16]. Ethanol (Merck, purity  $\geq 99.9\%$ ) and water were, respectively, contributed as the bore liquid and external coagulants. In order to obtain detailed data of outer layer tightness, H<sub>2</sub>, N<sub>2</sub> and helium were needed for reduction treatment and gas permeability test.

### 2.1.1 Fabrication of NiO–YSZ/LSCF–YSZ Dual-Layer Hollow Fiber Membrane

Co-extrusion which based on phase inversion method was applied using triple orifice spinneret to fabricate the dual-layer membrane and then was sequentially subjected to co-sintering as reported elsewhere [4]. The composition of NiO(60%)–YSZ(40%)/LSCF(30%)–YSZ(70%) was used in this study due to a high compatibility of each layer which is described elsewhere [5, 11].

The dope suspension of the inner and outer layers was firstly prepared separately in a calculated composition as mentioned in Table 1. NMP was poured and then LSCF, YSZ and PVP added gradually in a ball mill jar as an outer layer dope suspension. The inner layer was composed of NiO, YSZ and PVP. Both jars were milled at 183 rpm for 24 h and then PESf added into each suspension and milled again for 48 h to obtain high homogeneity. It was then degassed for an hour

**Table 2** The variation of bore liquid concentration and sintering temperature

Code	Bore liquid composition (v/v %)			Sintering temperature (°C)
	Water	Ethanol	NMP	
A2	100	–	–	1200
B2	40	10	50	
C2	25	25	50	
D2	–	100	–	
B3	40	10	50	1300
B4				1400
B5				1500
C3	25	25	50	1300
C4				1400
C5				1500

**Table 3** The sample name of the membrane after applying sintering and reducing treatment

Reduced membrane	Bore liquid composition (v/v %)			Sintering temp (°C)
	Water	Ethanol	NMP	
B3-R	40	10	50	1300
B4-R				1400
B5-R				1500
C3-R	25	25	50	1300
C4-R				1400
C5-R				1500

to remove air bubbles. Before extrusion process was applied, the viscosity of each dope suspension and bore liquid at certain composition was measured using Brookfield viscometer, DV-I Prime.

The extrusion parameter condition was controlled by syringe pumps (Harvard Apparatus, Holliston, MA). Furthermore, the sample name of different bore liquid concentration and sintering temperature are given in Table 2, while Table 3 represents the sample name of reduced membranes. Figure 2 illustrated the sintering profile for the membranes. The sintering temperature was varied at 1200, 1300, 1400 and 1500 °C using tubular furnace (URICH, UR-1700XY) to obtain a dense structure and high mechanical strength.

Since the membrane is potentially applicable to a POM reaction, a chemical bond breaking of Ni–O is required to obtain Ni by oxidation state O using a hydrogen reduction treatment. The membrane was inserted in the reactor, and the N<sub>2</sub> gas flowed through the reactor during a temperature rise from room temperature to 550 °C (5 °C min<sup>-1</sup>) to remove any potentially combustible gas impurities. Then, at 550 °C, H<sub>2</sub> gas flowed for 3 h. After that, the H<sub>2</sub> gas stream was changed

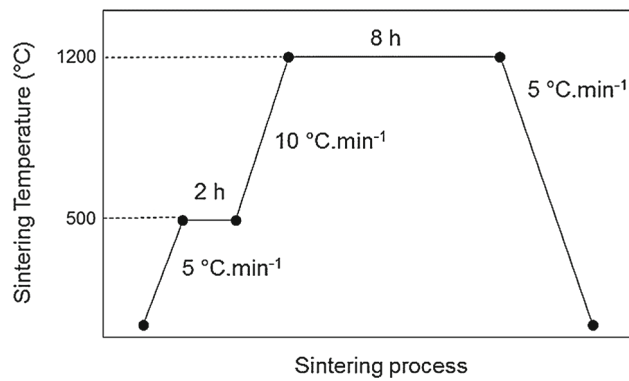


**Fig. 2** The sintering profile at sintering rate 5–10 °C min<sup>-1</sup>

to N<sub>2</sub> again during the temperature drop from 550 °C to room temperature. The unreduced and/or reduced membranes were then characterized to identify the morphology, membrane phase and performance of the N<sub>2</sub> gas tightness.

### 2.1.2 Characterization

The morphology and elements distribution in the membrane were identified using scanning electron microscopy–energy-dispersive X-ray (SEM, Hitachi TM-3000, Tokyo, Japan) and SEM–EDX (JEOL, ITBOOLV) for Y (L $\alpha$ , 1.9226 keV), Zr (L $\alpha$ , 2.0424 keV), Ni (L $\alpha$ , 0.8515 keV), La (L $\alpha$ , 0.8332 keV), Sr (L $\alpha$ , 1.8066 keV) [17]. Furthermore, a gas–liquid displacement technique using MicroActive AutoPore V 9600 version 1.03 at contact angle between mercury and the membrane surface of 130° was carried out.

The crystal structure of both layers was evaluated using X-ray diffraction (XRD). The reduced membrane layers of 1 mm were prepared on the zero background sample holder and then irradiated using with Cu K $\alpha$  ( $\lambda = 0.154178$  nm) at 30 kV and 15 mA as the X-ray source. Next, the diffraction was recorded at  $2\theta$  from 20° to 80° with a scan rate of 0.1° min<sup>-1</sup> and 0.02° step. Finally, the diffractogram was assigned by referring to the Joint Committee on the Powder Diffraction Standards (JCPDS) cards.

The three-point bending technique was used to measure the mechanical strength of the membrane using Instron Model 5567 tensile tester system with a crosshead speed of 1.0 mm min<sup>-1</sup> as performed by Mohamed et al. [5]. The membranes of with a measurement of 6 cm were taken of each parameter conditions for the average bending strength value and then loaded by 1 kN load cell as illustrated in Fig. 3 with the length of fixed sample holder (jig) of 43 mm. The maximum load of membrane fracture as  $F$  was recorded ( $N$ ) and then calculated using Eq. (1) to obtain the bending strength value ( $\sigma_f$ ) (MPa).

$$\sigma_f = \frac{8FLD_o}{\pi(D_o^4 - D_i^4)} \quad (1)$$

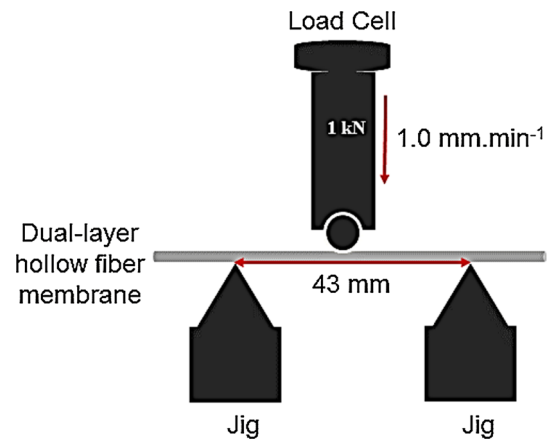


**Fig. 3** Three-point bending test illustration

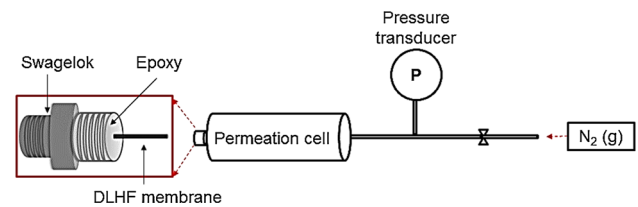


**Fig. 4** Setup for N<sub>2</sub> gas tightness test on dual-phase hollow fiber membrane

The length, outer diameter and inner diameter of the membrane are symbolized as  $L$ ,  $D_o$  and  $D_i$ , respectively (m) [18].

The membrane was also tested on N<sub>2</sub> gas tightness to identify and confirm the outer layer tightness at room temperature as illustrated in Fig. 4. The permeance of nitrogen leakage was examined in pressure change with time using Eq. (2) [19].

$$P = \frac{V}{RTA_m t} \ln \left( \frac{P_0 - P_a}{P_t - P_a} \right) \quad (2)$$

where  $P$  in mol m<sup>-2</sup> s<sup>-1</sup> Pa<sup>-1</sup> is the value of nitrogen permeation,  $V$  (m<sup>3</sup>) is the permeation cell volume of  $3 \times 10^{-5}$  m<sup>3</sup>,  $T$  is the temperature during the test in Kelvin,  $R$  is the gas constant value of 8.314 J mol<sup>-1</sup> K<sup>-1</sup>,  $P_0$  and  $P_t$  (Pa) are the initial and final pressures;  $P_a$  (Pa) is atmospheric pressure,  $t$  is the time of reduced nitrogen pressure from 3 to 1 Psi (s) and  $A_m$  (m<sup>2</sup>) is the effective membrane area which is calculated using following Eq. (3).

$$A_m = \frac{\pi(D_o - D_i)L}{\ln \left( \frac{D_o}{D_i} \right)} \quad (3)$$

where  $D_o$  and  $D_i$  in meter are, respectively, the outer and inner diameters of the membrane, and  $L$  (m) is the measured length of the membrane.

As a preliminary test, the certain membrane was then tested for the oxygen permeation using hollow fiber reac-

tor. Before the reaction, the membrane was reduced in H<sub>2</sub> atmosphere at 550 °C for 3 h to obtain Ni from NiO. Helium was used as the sweep gas during the test at a flow rate of 30 mL min<sup>-1</sup> and compressed air as the oxygen supplier of 150 mL min<sup>-1</sup>. The permeation was performed at 600, 700 and 800 °C; then, the data were recorded every 7 min at each temperature for 42 min using gas chromatography–thermal conductivity detector (GC-TCD), Buck Scientific Model 910. The oxygen permeates concentration which means the oxygen ion through the membrane ( $C_{O_2}^P$ ) (%) was calculated using Eq. (4) as follows:

$$C_{O_2}^P = C_{O_2}^r - C_{O_2}^l \tag{4}$$

where  $C_{O_2}^r$  is a recorded oxygen concentration in chromatogram and  $C_{O_2}^l$  is the oxygen concentration from the air (the probability of membrane leakage).

### 3 Results and Discussion

One of the primary prerequisites for dual-layer hollow fiber membrane fabrication using co-extrusion method is to determine the viscosity of the spinning suspension and bore liquid. In this present work, the value was recorded at shear rate from 2 to 60 s<sup>-1</sup> and collected at the certain shear rate of 50 s<sup>-1</sup>. As a result, the viscosity of NiO-YSZ (inner layer) was 3978.7 cP while LSCF-YSZ (outer layer) was relatively lower at 538.8 cP as shown in Fig. 5. The difference between the two viscosity values in both spinning suspensions greatly influenced the layer membrane structure and formation during extrusion process. The greater viscosity of the inner layer spinning suspension leads to the high compatibility membrane which can be used as a support. It is due to a high viscosity of the suspension that showed greater mechanical strength as reported previously [8, 19]. It was then successfully coated with the less viscous suspension on the outer layer. In addition, benefiting from the higher viscosity of inner layer than outer layer suspension is to achieve great

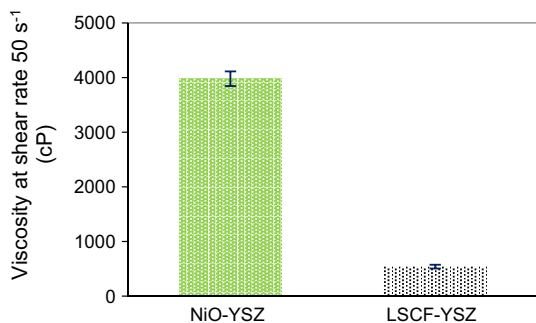


Fig. 5 The viscosity of dope suspensions at three repetitions on measurements

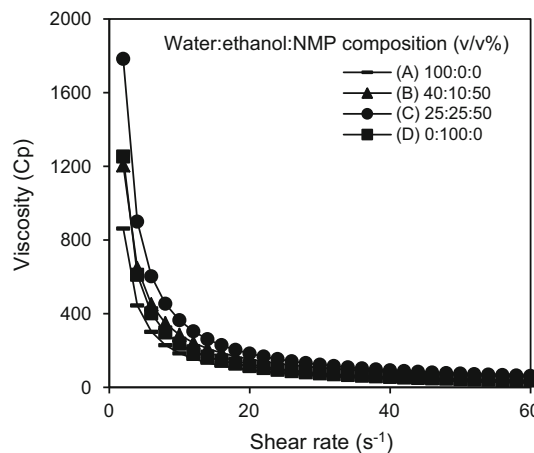


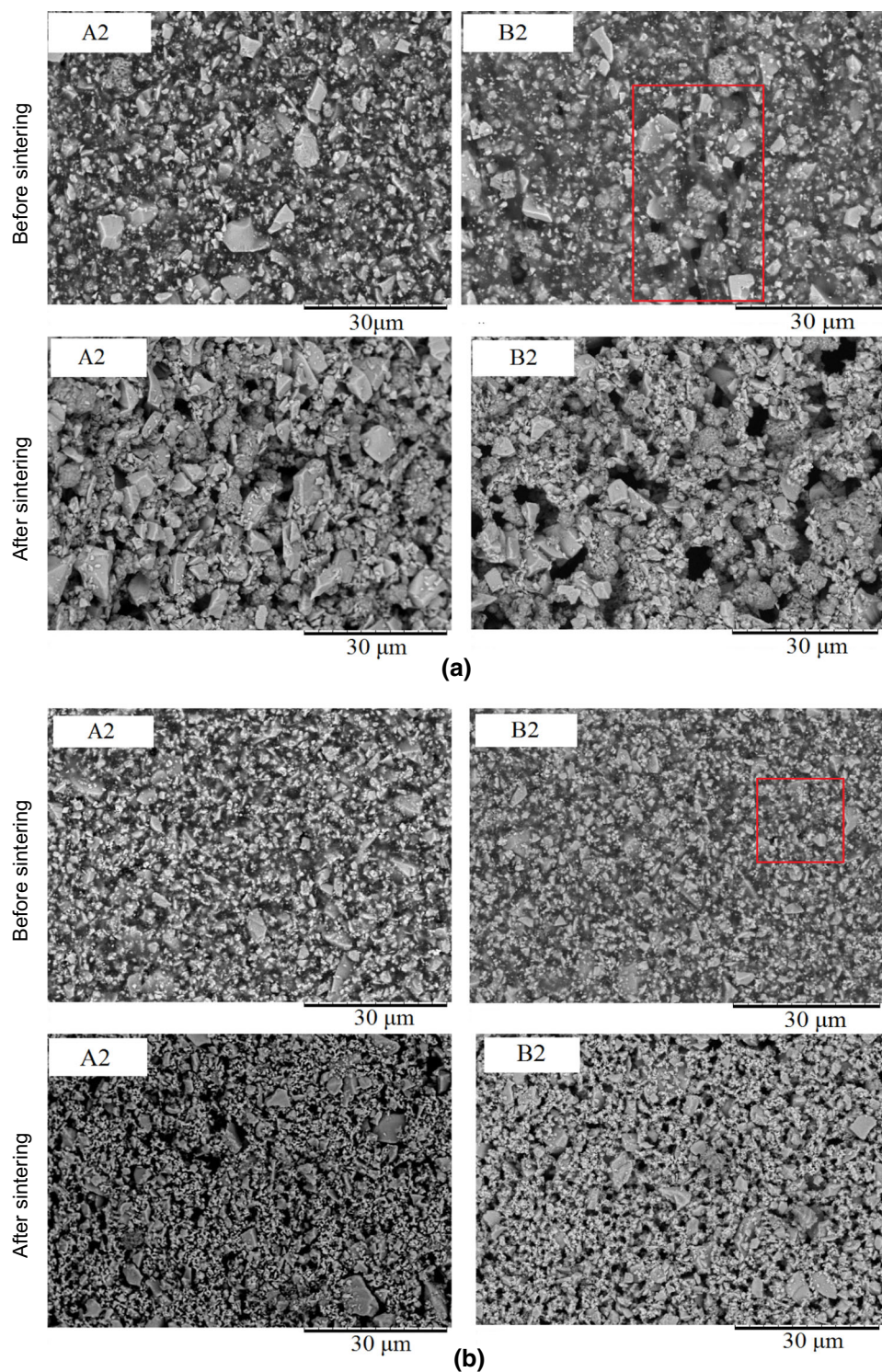
Fig. 6 Viscosity of different water/ethanol/NMP composition as a bore liquid

adhesion and good interconnection between two layers to avoid membrane delamination which initiate damage and finally decrease the membrane performance, especially for high-temperature application.

Furthermore, the viscosity of the bore liquid was also measured in order to evaluate the internal resistance value and the speed of movement of bore liquid during co-extrusion step, either on pure or mixed bore liquid. As shown in Fig. 6, the rheological profiles show the viscosity of water/ethanol/NMP in different compositions v/v %. The obtained patterns show the similar behavior as the results reported by Paiman et al. [20], that is the increase in shear rate decreases the viscosity value; however, at the certain shear rate (60 s<sup>-1</sup>), the viscosity value started to remain constant. The lowest viscosity was attained by 100% water at approximately 39.77 cP and followed by the 100% ethanol which was at 44.50 cP. By addition of NMP and ethanol in water at the composition of water (40%)/ethanol (10%)/NMP(50%), the viscosity further increased at approximate value of 67.40 cP and then slightly increase up to 74.38 cP with the increase of the ethanol content (water (25%)/ethanol (25%)/NMP (50%)).

The varied bore liquid composition showed different appearance, for instance, 100% water revealed clear liquid with no air bubbles as well as the bore liquid with 100% ethanol. Conversely, the mixed bore composition produced air bubbles which affect the flow of spinning suspension during co-extrusion process. This is due to the air bubbles that provide an empty gap of the bore liquid which breaks the membrane precursor during the extrusion process and thus deteriorates the membrane such as breaking the membrane precursor and decreasing pore regularity. Therefore, the bore liquid rate should be determined to ensure the smooth flow of the spinning process and obtain a well-rounded and

**Fig. 7** SEM micrograph of the inner (A) and outer (B) surfaces of the membrane before (a) and after (b) sintering process at 1200 °C



fully covered dual-layer membrane at the bore liquid rate of 8–12 mL min<sup>-1</sup>.

The effect of 100% water, the mixture liquid (water, ethanol, NMP) and 100% ethanol as bore liquid on the inner and outer surface structures of the membrane can be seen in Fig. 7. Overall, the inner layer surface of the membrane is

more porous than the outer layer surface. It was found in the membrane precursor that pore was shown as signed (the red square) on the outer layer surface of membrane B2 while the outer layer surface of A2 membrane is tighter. This reveals that the evaporation of ethanol from the inside to the outside of the membrane occurs during the spinning process.

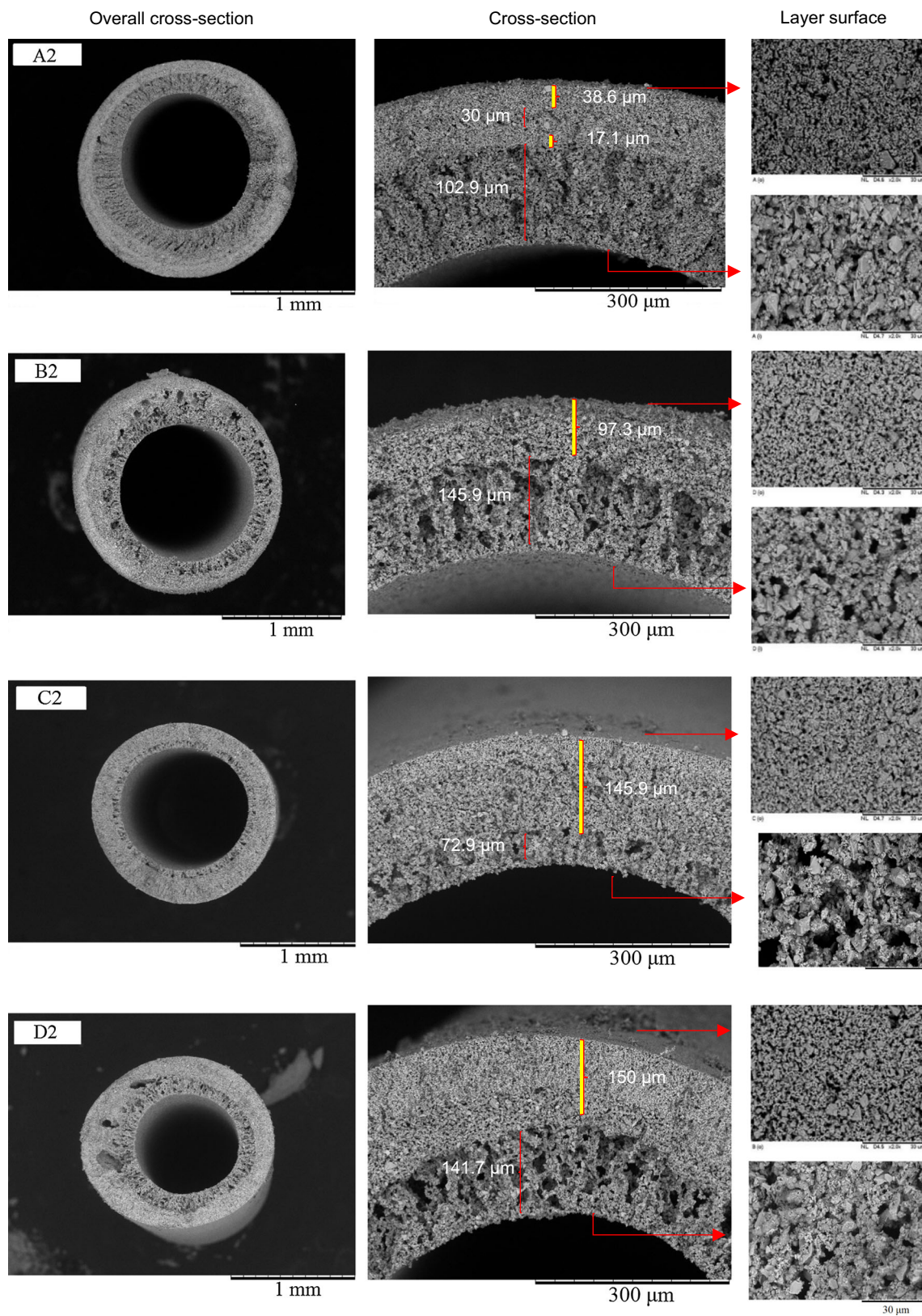


**Fig. 8** SEM micrograph of the overall cross section, half cross section, outer and inner surfaces of NiO-YSZ/LSCF-YSZ with different bore liquid sintered at 1200 °C

The consolidation of the membrane precursor was carried out by the co-sintering method at 1200 °C for 8 h. The pore size of membrane A2 shows denser structure than the membrane B2. This pore formation on the membrane surface indicates the disappearance of the ceramic powder at high temperatures so that the precursor particles are closer to form a larger and denser grain.

The SEM images of the obtained membrane are presented in Fig. 8. Generally, there are two kinds of pore structure: sponge-like and finger-like. When water was used as the internal and external coagulants, membrane A2 shows finger-like pore in both inner and outer layers (sandwich-like) which may lead to a decrease in oxygen permeation 2.6–10.5 times as reported by Wang et al. [21]. This is due to the increase in oxygen ion diffusion travel time from outer to inner layer membrane, according to the barrier layer (dense) between finger-like pore in both layers.

On the contrary, membranes B2, C2 and D2 show similar pore configuration of finger-like pore in inner edge and sponge-like in outer edge. It relates to the bore liquid viscosity information with pore formation. The more viscous bore liquid caused by NMP addition leads to decrease in the polymer precipitation in NMP. It simultaneously decreased the exchange rate between solvent and non-solvent; thus, the longer pores (finger-like) can be formed as observed in previous study [8]. As the amount of water/ethanol/NMP is 40%:10%:50% in membrane B2, the sponge-like (dense) thickness is reduced which indicates that the ethanol mostly dissolved in water and NMP. On the other hand, the different v/v % ratio in a mixture of bore liquid affects the thickness (145.95  $\mu\text{m}$ ) of dense layer in membrane C2, which was thicker than B2 (97.29  $\mu\text{m}$ ). In addition, the parts of membrane C2 broke off several times during spinning process. It was affected by the mixture 25 v/v % ethanol in water and NMP. It indicates that this mixture composition in the bore liquid was not appropriate to be used as a bore liquid. This was confirmed by Innocenzi et al. [22] that binary and single solution in the membrane was evaporated at different times which depends on the composition of the mixture.

The SEM image also confirms that the sponge-like of D2 (150  $\mu\text{m}$ ) is longer than A2 (38.57  $\mu\text{m}$ ), but a high uniform finger-like configuration with small dense thickness is formed in membrane B2. In addition, the use of 100 v/v % ethanol in membrane D2 forms more finger-like pore at the inner surface than 100% pure water of membrane A2. It also revealed that finger-like pore formation at the inner surface in water and NMP mixture of B2 and C2 is significantly decreased with increasing ethanol addition in a bore liquid mixture. It confirms that ethanol in C2 is easily evaporated than in B2. The outer surface also shows pore when ethanol was added in the bore liquid. It indicates that ethanol also diffuses pass through to the outer surface of membranes and then evaporates into the air.

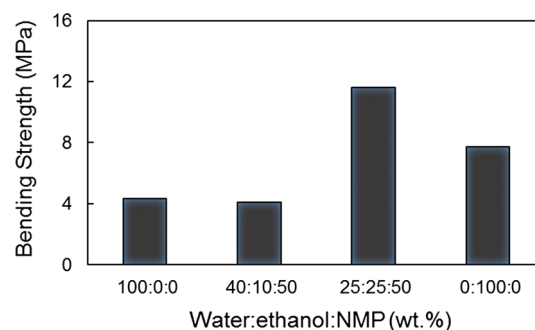


Fig. 9 The mechanical strength of membrane A2, B2, C2 and D2 at sintering temperature of 1200 °C

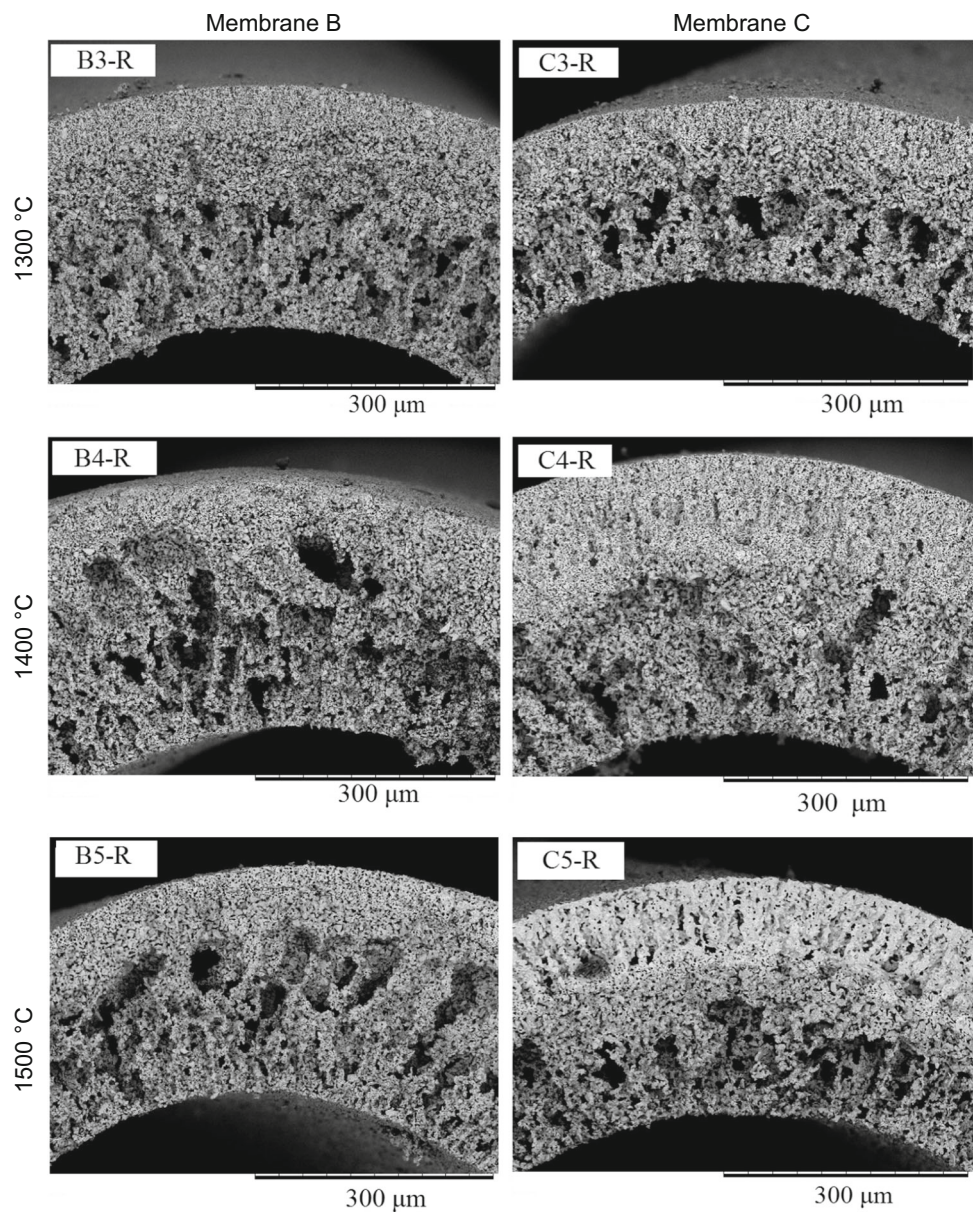
The mechanical strength was further measured to examine the physical stability of the membrane [23]. As shown in Fig. 9, the hollow fiber fabrication using pure water as a bore liquid shows higher bending strength than 10 v/v % ethanol which confirmed that a high bending strength of A2 is caused by sandwich pore configuration where the barrier layer increases the mechanical strength slightly. Meanwhile, the membrane C2 (25 v/v % ethanol) possess highest mechanical strength of 11.63 MPa, which correlate with the regular pore configuration and higher dense layer (sponge-like pore).

Due to the low mechanical strength of the membranes, the sintering at higher temperature is systemically applied to achieve high mechanical strength and tightness to  $\text{N}_2$  gas. The existence of  $\text{N}_2$  shows that the membrane leaks and it leads to the reaction between methane and  $\text{N}_2$  and/or  $\text{O}_2$  during POM reaction to form undesired products such as carbon deposition,  $\text{NO}_x$  and  $\text{CO}_2$ . In addition, the reduction process after sintering was employed in membranes at higher sintering temperature of 1300, 1400 and 1500 °C. The reduction treatment is absolutely vital which means POM reaction is highly activated and more favorable in the form of Ni with oxidation state of 0. The reduced membrane was changed to be more porous which caused decreasing oxygen content in Ni–O as probed by Wu et al. [24].

Figure 10 shows the final membrane morphology in cross section of membranes B and C which were co-sintered at 1300, 1400 and 1500 °C and reduced using  $\text{H}_2$ . Membranes B and C have been used for further investigation of the properties after applying higher sintering temperature as mentioned due to the arrangement of pore configuration of sponge-like configuration in the outer edge with integrated finger-like configuration in the inner edge at the sintering temperature of 1200 °C which was in accordance with the promoted design in this study. The membranes B3-R, B4-R, B5-R and C3-R exhibited asymmetrical structure with finger-like configuration originating from inner layer and become denser toward the outer layer.



**Fig. 10** SEM micrograph of sintered membrane at 1300, 1400 and 1500 °C and reduced in H<sub>2</sub> atmosphere at 550 °C



On the other hand, barrier sponge-like pore structure is significantly seen on C4-R and C5-R membranes. It confirms that 25 v/v % ethanol addition in C membrane is easily evaporated to the environment even at room temperature before solidification process was occurred. Hence, when the membrane is immersed in water as external coagulant, the exchange rate between solvent and non-solvent on outer surface is close to the exchange rate on the inner surface, due to water content in the mixture of bore liquid, while the ethanol was evaporated. Thus, the membrane pore turns into sandwich-like structure as shown in mentioned figure. This process certainly occurred in the precipitation phase of polymeric solution and the solvent–non-solvent, as described in ternary phase diagram by Ahmad et al. [25].

The identifiable sandwich-like pore in membrane C is shown clearly at high sintering temperature of 1400 and 1500 °C. The increase in the sintering temperature also reveals rougher macro-voids which is caused by the decrease in oxygen of NiO in inner layer and the increase in the particle interconnected simultaneously. However, a uniform pore configuration with high consistency is achieved by B3-R membrane, although reducing process was applied.

Figure 11 represents inner and outer surfaces of membranes B and C. As the sintering temperature is further increased, both inner and outer surfaces are extremely dense. It indicates that the increase in sintering temperature produced more compact interconnection in the particles thus forming more closed surface.

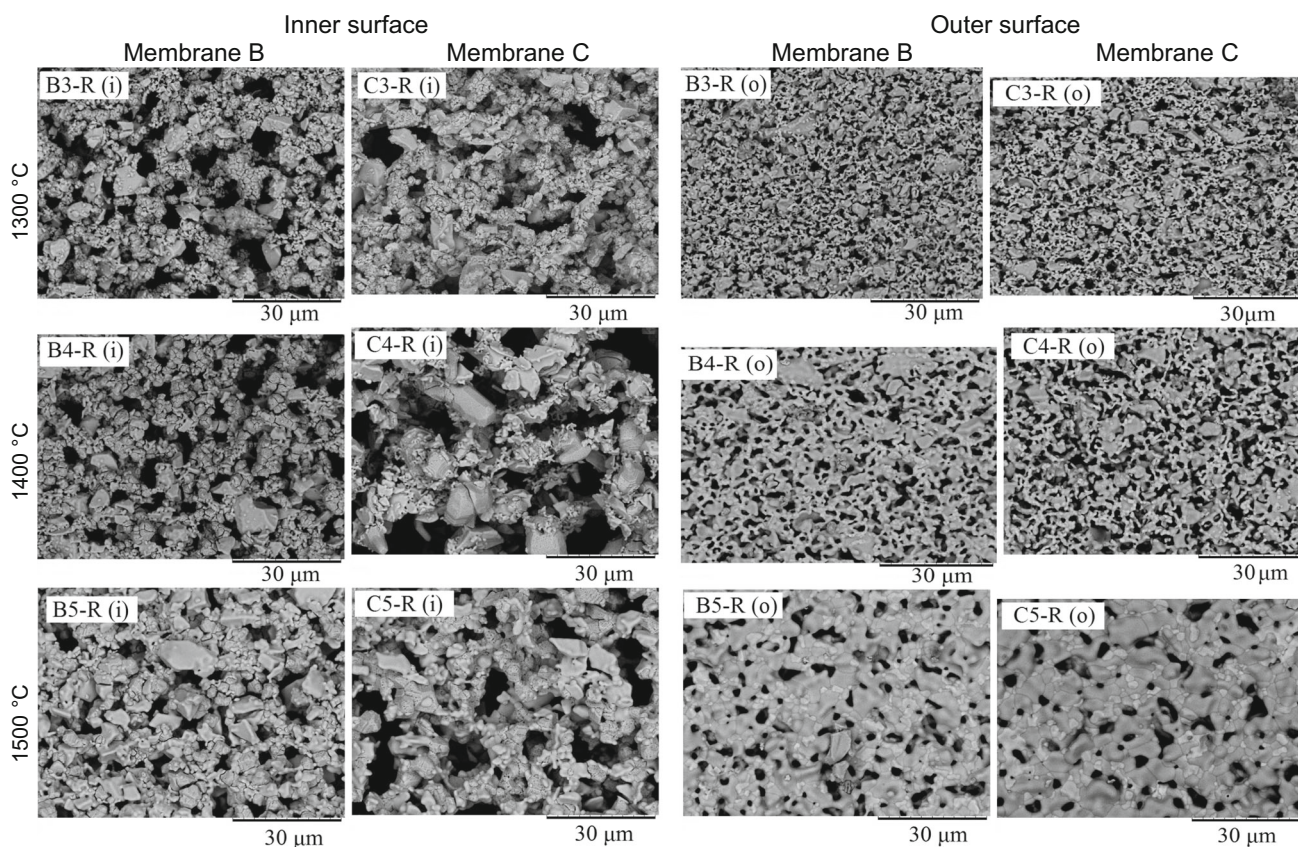


**Fig. 11** SEM micrograph of the inner and outer membrane surfaces after sintering and reducing

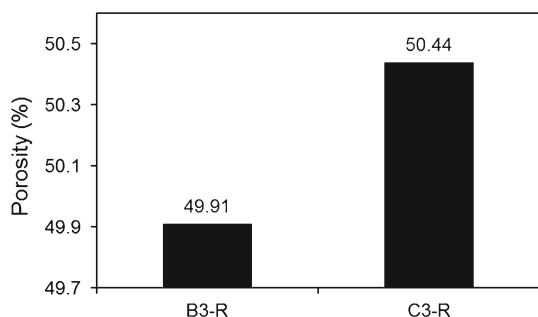


**Fig. 12** The porosity of membrane B3-R and C3-R

Figure 12 presents the effect of different bore liquid ratios on the membrane porosity using mercury intrusion porosimetry (MIP) analysis. It was found that the porosity value of membrane B3 at 49.91% which slightly smaller than membrane C3 of 50.44% supported the SEM image as described above.

For further study, Fig. 13 clearly shows the pore size distribution (Dp) curve, representing asymmetric micro-structure formation in membrane B3-R and C3-R. Membrane B3 exhibited more regular pore configuration and bigger sponge-like size with pore diameter ranging from 0.1 to 8 nm than membrane C3 with pore diameter between 0.1 and 0.08 nm.

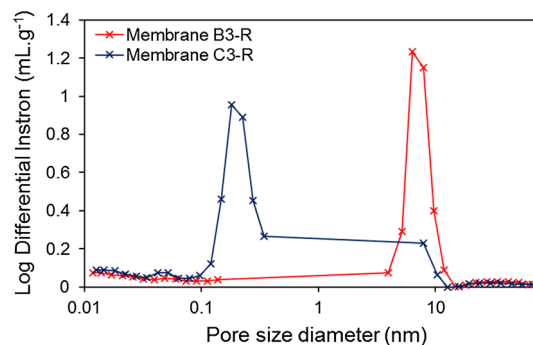


**Fig. 13** The pore size diameter of the membranes

In addition, membrane C3-R with higher ethanol content was found to have macro-void pore and smaller finger-like pore opening size diameter from 0.1 to 11 nm, while the membrane B3-R showed less broadening at approximately 8 to 12 nm pore size. This indicates that the increase in ethanol initiates more varied size of finger-like pore; thus, it initiates different membrane properties.

The schematic diagrams as shown in Fig. 14 illustrated the effect of the different bore liquid composition on the pore configuration formation in dual-layer hollow fiber membrane. Principally, the pore formation in

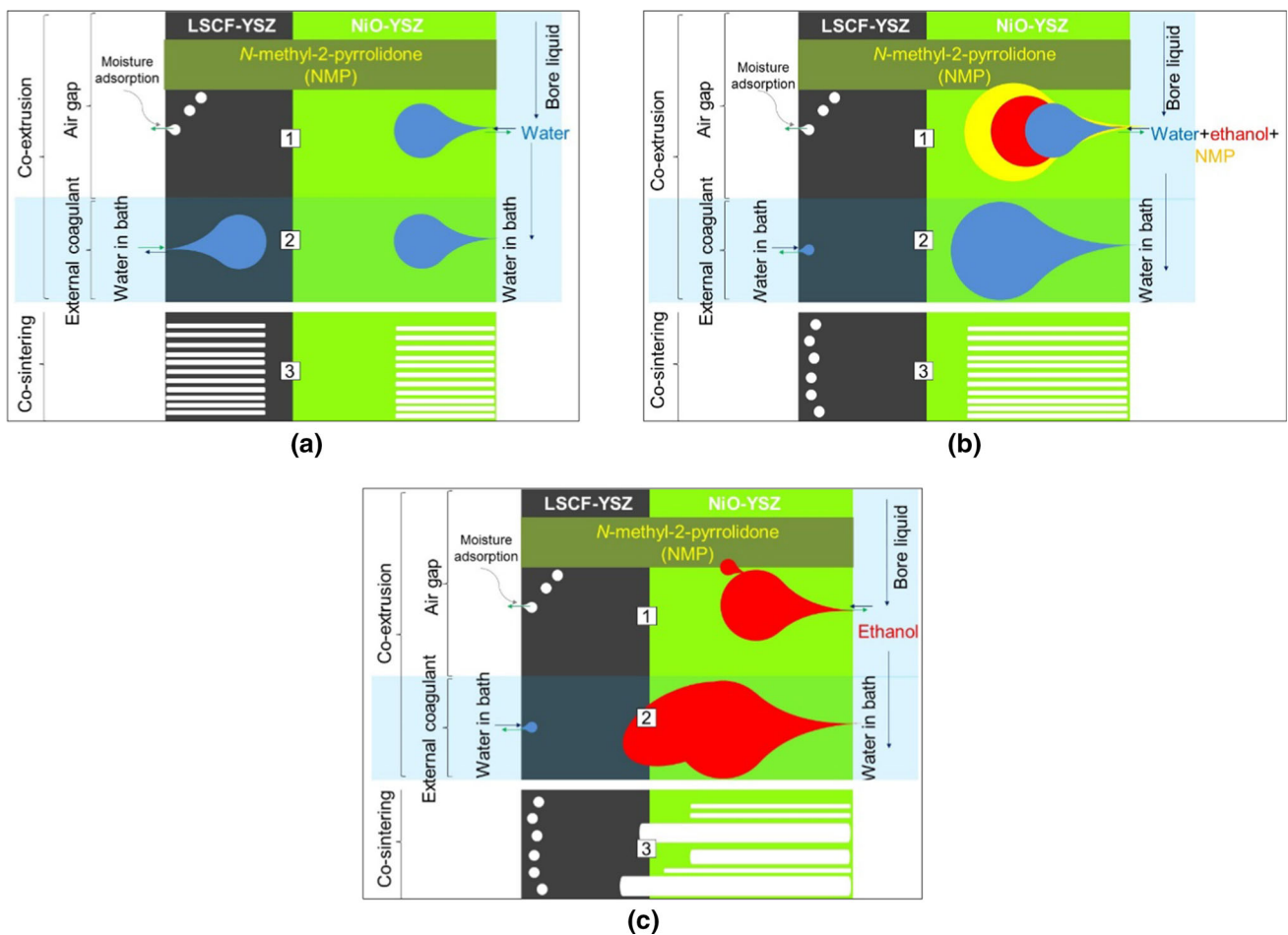


**Fig. 14** The illustration of adsorption, diffusion and exchange process between solvent and non-solvent in the membrane during co-extrusion and co-sintering process [Green color: inner layer (NiO-YSZ) and black color: outer layer (LSCF-YSZ)]

phase inversion technique includes four major steps: adsorption, diffusion of coagulant solution, exchange between solvent and coagulant solution [26], and pore formation. The pore formation is mainly influenced by the diffusion velocity and the exchange rate between solvent and non-solvent.

The process begins with the moisture adsorption process from the air to the outer membrane so that the sponge-like pore is more dominantly formed while the adsorption of bore liquid earlier occurs to form the finger-like pore through the nascent fiber. As can be seen in Fig. 8a, the water as bore liquid tends to form a sandwich-like pore due to the same exchange rate in both layers. This pore configuration has a weakness that can block the permeation of oxygen across the membrane. On the contrary, ethanol becomes the most preferred liquid to form finger-like pore because the diffusion velocity is greater than water as external coagulant. However, the handling of ethanol as a bore liquid has its own complexity because it is easily evaporated at room temperature so that the pores formed can not be controlled and produced greater

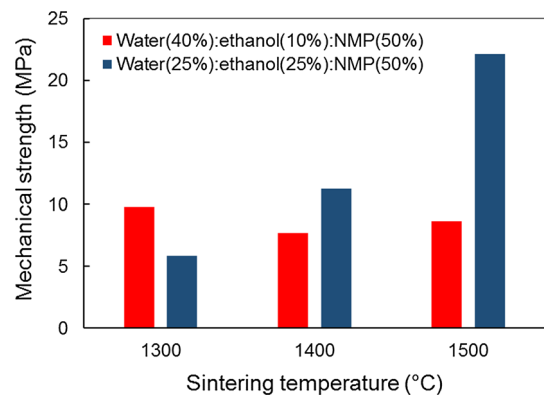
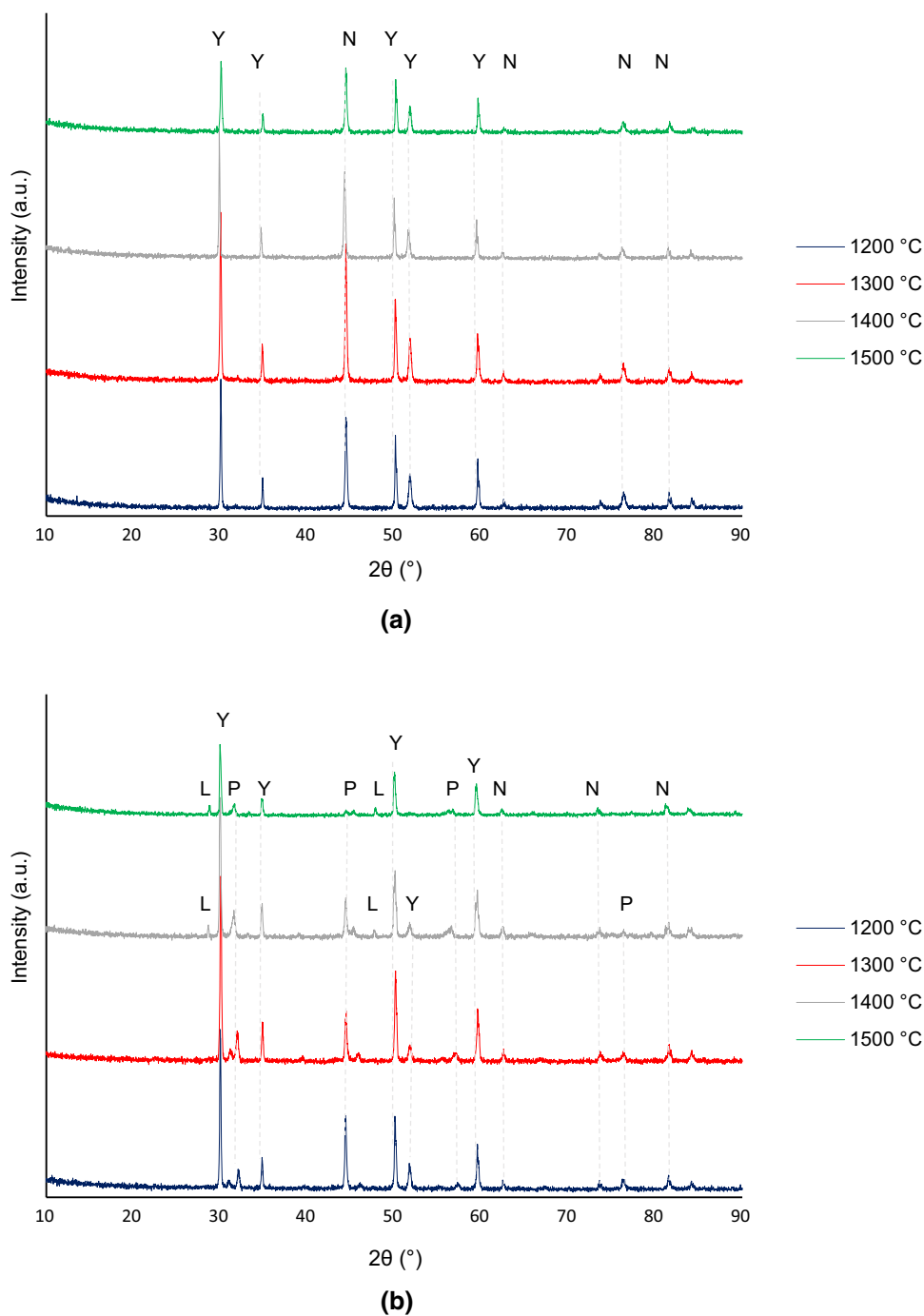


**Fig. 15** The bending strength of membrane B [water(40%)/ethanol(10%)/NMP(50%)] and membrane C [water(25%)/ethanol(25%)/NMP(50%)] at different sintering temperature

pore volume which leads to irregularity and macro-voids pore configuration.

The use of NMP mixed in water and ethanol increases the diffusion velocity to the membrane. As previously explained

**Fig. 16** The diffractogram of inner (a) and outer (b) layers reduced membranes at different sintering temperatures (Y: YSZ, N: Ni, P: LSCF and L:  $\text{La}_2\text{Zr}_2\text{O}_7$ )



ethanol and NMP increase the viscosity. A similar viscosity involved high attraction and then ethanol and water mobilize into the membrane to form pores. As a result, the evaporation of ethanol can be controlled by the addition of water. Tan et al. [8] explained that the use of NMP and ethanol increased the rate of diffusion to avoid the formation of sandwich-like morphology. Thus, the pore forms finger-like structure on the inside and sponge-like structure on the outside of the membrane with high regularity using a mixture of water/ethanol/NMP.

Based on the bending strength result in Fig. 15, B3 with high regular finger-like pore structure and no macro-voids defect exhibits higher bending strength compared to the membranes B4, B5 and D3, while that of the membranes D4 and D5 dramatically increased. At this stage, it was almost certain that the mechanical strength can be related to the pore formation in the membrane.

In order to identify the chemical properties of the membranes especially phase stability of NiO, YSZ and LSCF, the XRD was applied to record the significant phase changes

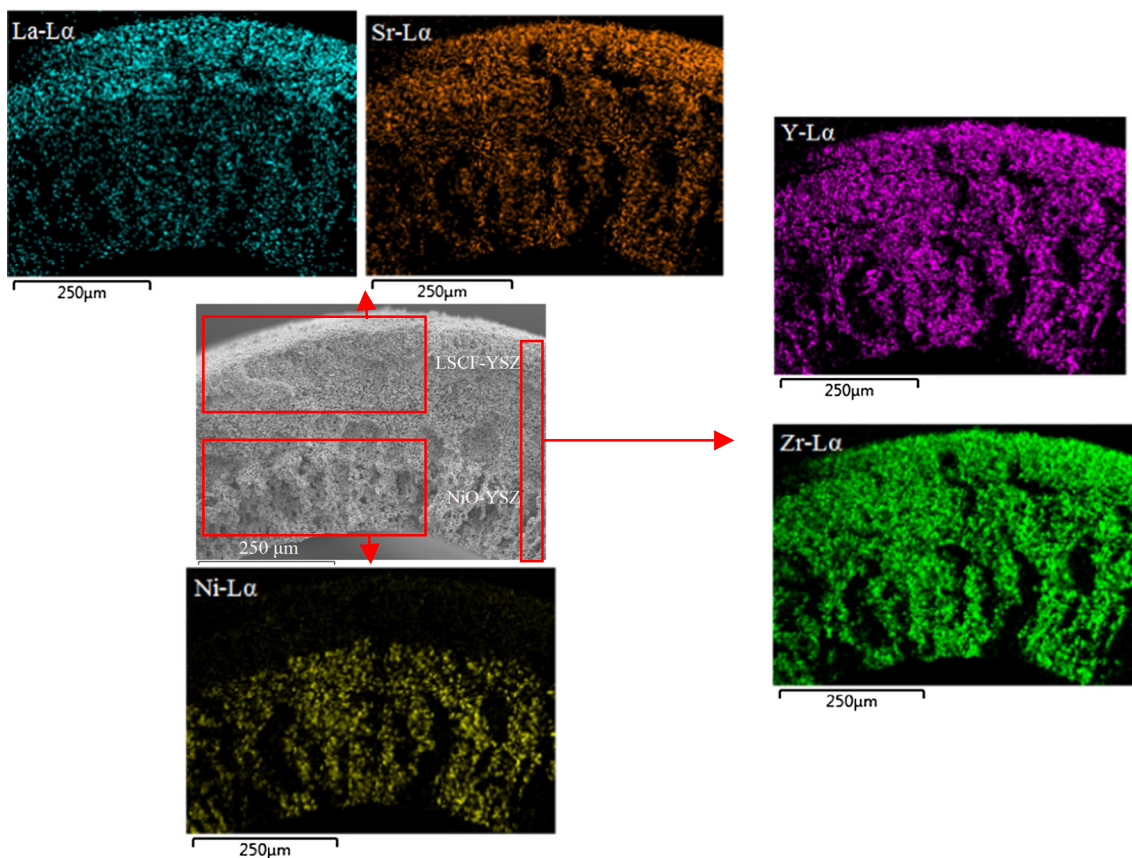


**Fig. 17** SEM-EDX images of concentration mapping of principal elements of B3-R

at each layer as the diffractogram shown in Fig. 16. The phase crystallinity at inner and outer layers decreased with the increase in the temperature. The inner layer phase remains unchanged, and there is no impurity phase formation even up to 1500 °C, while the NiO peak shows a shift to a larger  $2\theta$ . It indicates the decrease in the NiO crystal size at the higher sintering temperature. This differs from the diffractogram at the outer layer membrane which is composed of LSCF and YSZ composites. At the sintering temperature of 1400 and 1500 °C reveals an impurity phase in the form of  $\text{La}_2\text{Zr}_2\text{O}_7$  (PDF: 00-071-2363) around  $2\theta$ : 28° and 48°. Therefore, the sintering temperature at 1300 °C shows a low level of impurity phase which maintains the stability of material functions in the membrane form.

To gather more information about the material after applying different bore liquid and sintering temperature, it is extremely important to observe the elemental distribution within layers along membrane cross section using SEM–EDX. Figure 17 shows the elements distribution across of 300–400 μm active inner (NiO-YSZ) and outer (LSCF-YSZ) layers with finest grain size. Ni on both membranes was well separated in the inner layer, while Y and Zr are distributed uniformly in both layers. This shows that YSZ works well as a separator between the Ni and LSCF layers

and helps prevent the diffusion of Ni into the LSCF layer without compromising the oxygen diffusion from LSCF to Ni layers.

Considering the different elemental composition at both layers, the elemental distribution is highly important to identify the membrane formation [27]. The SEM-EDX images show that LSCF elements, which should be in the outer layer, was also found in the Ni (inner) layer. Nevertheless, in an approximation of EDX result, strontium and lanthanum are mostly found in outer layer of the dual-layer membrane with no significant differences. Thus, it can be proposed that 1300 °C and 8 h is the optimum sintering condition, based on the membrane morphology and elemental identification.

The sintering process is the last step on membrane fabrication, but it has highly critical analysis to ensure the membrane still has good characteristics especially nitrogen tightness after reduction treatment to be applied for POM catalyst. Although Wang et al. [21] reported that around 0.1–1.8% nitrogen was assumed to be leaked than distributed through the membrane. The nitrogen tightness was then performed on the obtained membrane as the preliminary performance test of the membrane. Figure 18 shows that the nitrogen permeability decreases with the increase in the sintering temperature with the lowest value which has been achieved using

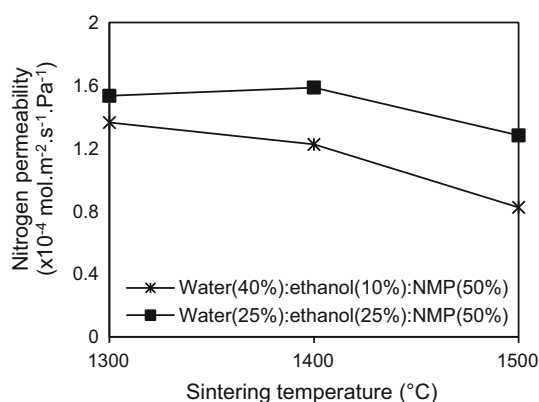


**Fig. 18** N<sub>2</sub> gas permeability of membranes B and C at different sintering temperatures

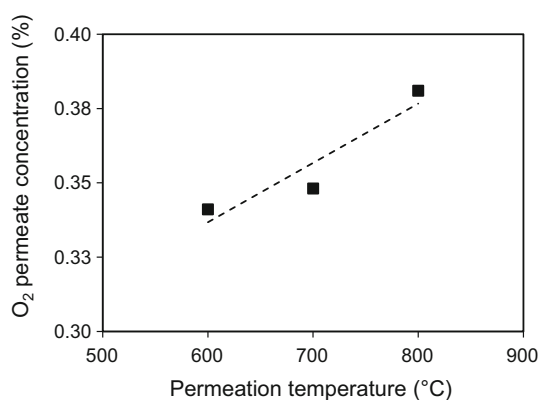


**Fig. 19** Oxygen permeate concentration at different permeation temperatures of membrane B3-R

B5 membrane. This phenomenon may be due to the higher sintering temperature which increased the outer surface density. However, such increase in ethanol as bore liquid over a mixture of water + NMP with high mechanical strength in form of C3 membrane shows higher value as compared to the B3 membrane.

Hence it can be correlated with outer surface micrograph in Fig. 11 which gives denser surface than the surface of membrane C3. In addition, the presence of higher finger-like regularity and lower macro-voids reduced the nitrogen gas diffusion from outer to inner membrane.

Figure 19 shows oxygen permeate concentration as a function of temperature of 600, 700 and 800 °C using 30 mL min<sup>-1</sup> helium flow rate. As expected, the O<sub>2</sub> permeate concentration was slightly lower than single layer of LSCF hollow fiber membrane as reported by Tan et al. [28]. One of the possible reasons is the different membrane layer. In addition, the presence of unreduced NiO into Ni in inner layer may lead the oxygen mass transfer resistance. Eventually, the O<sub>2</sub> permeate concentration in the lumen was reduced. A further driving force was then applied such as the temper-

ature from 600 to 800 °C. The O<sub>2</sub> permeate concentration dramatically increased with the increase in temperature.

## 4 Conclusion

As the apparent result, a bore liquid and the sintering temperature affect the dual-layer catalyst membrane properties especially morphological configuration and elemental distribution of NiO–YSZ/LSCF–YSZ. The mixture of ethanol, water and NMP shows arranged finger-like pore integrated with sponge-like pore, from inner layer to the outer layer. The increase in ethanol of 25% in water and NMP increases sponge pore length as ethanol is easily evaporated at room temperature. The developed characteristic of dual-layer hollow fiber membrane with high pore consistency was achieved using 40:10:50% water:ethanol:NMP as a bore liquid mixture and applying the co-sintering temperature of 1300 °C for 8 h. In addition, the oxygen ion permeability of the dual-layer hollow fiber membrane was slightly lower than the previously reported oxygen permeability using single-layer membrane. As a further performance improvement, highly dense membranes can be produced using smaller particle sizes and modulating the composition of the outer layer material to limit the distribution of elements in both layers, producing membranes with high compactness and preventing membranes from delamination.

**Acknowledgements** This study was financially supported by Directorate General of Higher Education, Indonesian Ministry of Research, Technology and Higher Education in the form of PMDSU scholarship and research grant with contract number 128/SP2H/PTNBH/DRPM/2018. The authors would also like to thank Advanced Membrane Technology Research Centre (AMTEC), School of Chemical and Energy Engineering, Universiti Teknologi Malaysia for the technical support.

## References

- Shelepova, E.; Vedyagin, A.; Sadykov, V.; Mezentseva, N.; Fedorova, Y.; Smorygo, O.; Klenov, O.; Mishakov, I.: Theoretical and experimental study of methane partial oxidation to syngas in catalytic membrane reactor with asymmetric oxygen-permeable membrane. *Catal. Today* **268**, 103–110 (2016)
- Tan, X.; Liu, Y.; Li, K.: Preparation of LSCF ceramic hollow-fiber membranes for oxygen production by a phase-inversion/sintering technique. *Ind. Eng. Chem. Res.* **44**, 61–66 (2005)
- Dai, X.; Yu, C.; Wu, Q.: Comparison of LaFeO<sub>3</sub>, La<sub>0.8</sub>Sr<sub>0.2</sub>FeO<sub>3</sub>, and La<sub>0.8</sub>Sr<sub>0.2</sub>Fe<sub>0.9</sub>Co<sub>0.1</sub>O<sub>3</sub> perovskite oxides as oxygen carrier for partial oxidation of methane. *J. Nat. Gas Chem.* **17**, 415–418 (2008)
- Wu, Z.; Wang, B.; Li, K.: A novel dual-layer ceramic hollow fibre membrane reactor for methane conversion. *J. Memb. Sci.* **352**, 63–70 (2010)
- Mohamed, M.H.; Othman, M.H.D.; Abd Mutalib, M.; Rahman, M.; Jaafar, J.; Ismail, A.F.; Dzahir, M.I.H.: Structural control of NiO–YSZ/LSCF–YSZ dual-layer hollow fiber membrane for

- potential syngas production. *Int. J. Appl. Ceram. Technol.* **13**, 799–809 (2016)
6. Witte, P.; Dijkstra, P.J.J.; Berg, J.W.; Feijen, J.: Phase separation processes in polymer solutions in relation to membrane formation. *J. Memb. Sci.* **117**, 1–31 (1996)
  7. Li, L.; Chen, M.; Dong, Y.; Dong, X.; Cerneaux, S.; Hampshire, S.; Cao, J.; Zhu, L.; Zhu, Z.; Liu, J.: A low-cost alumina-mullite composite hollow fiber ceramic membrane fabricated via phase-inversion and sintering method. *J. Eur. Ceram. Soc.* **36**, 2057–2066 (2016)
  8. Tan, X.; Liu, N.; Meng, B.; Liu, S.: Morphology control of the perovskite hollow fibre membranes for oxygen separation using different bore fluids. *J. Memb. Sci.* **378**, 308–318 (2011)
  9. Tan, X.; Shi, L.; Hao, G.; Meng, B.; Liu, S.:  $\text{La}_{0.7}\text{Sr}_{0.3}\text{FeO}_{3-\alpha}$  perovskite hollow fiber membranes for oxygen permeation and methane conversion. *Sep. Purif. Technol.* **96**, 89–97 (2012)
  10. Yang, N.T.; Kathiraser, Y.; Kawi, S.: A new asymmetric  $\text{SrCo}_{0.8}\text{Fe}_{0.1}\text{Ga}_{0.1}\text{O}_{3-\delta}$  perovskite hollow fiber membrane for stable oxygen permeability under reducing condition. *J. Memb. Sci.* **428**, 78–85 (2013)
  11. Li, K.; Tan, X.; Liu, Y.: Single-step fabrication of ceramic hollow fibers for oxygen permeation. *J. Memb. Sci.* **272**, 1–5 (2006)
  12. Shao, Z.; Xiong, G.; Cong, Y.; Yang, W.: Synthesis and oxygen permeation study of novel perovskite-type  $\text{BaBi}_x\text{Co}_{0.2}\text{Fe}_{0.8-x}\text{O}_{3-\delta}$  ceramic membranes. *J. Memb. Sci.* **164**, 167–176 (2000)
  13. Park, S.; Choi, S.; Kim, J.; Shin, J.; Kim, G.: Strontium doping effect on high-performance  $\text{PrBa}_{1-x}\text{Sr}_x\text{Co}_2\text{O}_{5+\delta}$  as a cathode material for IT-SOFCs. *ECS Electrochem. Lett.* (2012). <https://doi.org/10.1149/2.007205eel>
  14. Nurherdiana, S.D.; Sholichah, N.; Iqbal, R.M.; Sahasrikirana, M.S.; Utomo, W.P.; Akhlus, S.; Fansuri, H.: Preparation of  $\text{La}_{0.7}\text{Sr}_{0.3}\text{Co}_{0.2}\text{Fe}_{0.8}\text{O}_{3-\delta}$  (LSCF 7328) by combination of mechanochemical and solid state reaction. *Key Eng. Mater.* **744**, 399–403 (2017)
  15. Iqbal, R.M.; Nurherdiana, S.D.; Sahasrikirana, M.S.; Harmelia, L.; Utomo, W.P.; Setyaningsih, E.P.; Fansuri, H.: The compatibility of  $\text{NiO}$ ,  $\text{CeO}_2$  and  $\text{NiO-CeO}_2$  as a Coating on  $\text{La}_{0.6}\text{Sr}_{0.4}\text{Co}_{0.2}\text{Fe}_{0.8}\text{O}_{3-\delta}$ ,  $\text{La}_{0.7}\text{Sr}_{0.3}\text{Co}_{0.2}\text{Fe}_{0.8}\text{O}_{3-\delta}$  and  $\text{La}_{0.7}\text{Sr}_{0.3}\text{Mn}_{0.3}\text{O}_{3-\delta}$  ceramic membrane and their mechanical properties. *IOP Conf. Ser. Mater. Sci. Eng.* (2018). <https://iopscience.iop.org/article/10.1088/1757-899X/367/1/012032>. Accessed 31 Jan 2019.
  16. Chi, Y.; Li, T.; Wang, B.; Wu, Z.; Li, K.: Morphology, performance and stability of multi-bore capillary  $\text{La}_{0.6}\text{Sr}_{0.4}\text{Co}_{0.2}\text{Fe}_{0.8}\text{O}_{3-\delta}$  oxygen transport membranes. *J. Memb. Sci.* **529**, 224–233 (2017)
  17. Sajidah, H.B.N.; Nurherdiana, S.D.; Utomo, W.P.; Iqbal, R.M.; Hartanto, D.; Othman, M.H.D.; Fansuri, H.: Preparation and characterization of dual-layer hollow fibre catalyst membrane for oxygen transport. *AIP Conf. Proc.* (2018). <https://aip.scitation.org/doi/abs/10.1063/1.5082495>. Accessed 31 Jan 2019
  18. Wit, P.; Daalen, F.S.; Benes, N.E.: The mechanical strength of a ceramic porous hollow fiber. *J. Memb. Sci.* **524**, 721–728 (2017)
  19. Othman, M.H.D.; Droushiotis, N.; Wu, Z.; Kelsall, G.; Li, K.: Dual-layer hollow fibres with different anode structures for micro-tubular solid oxide fuel cells. *J. Power Sources* **205**, 272–280 (2012)
  20. Rahman, M.A.; Ha, M.; Othman, D.; Ismail, A.F.: Morphological study of yttria-stabilized zirconia hollow fibre membrane prepared using phase inversion/sintering technique. *Cer. Int.* **41**, 12543–12553 (2015)
  21. Wang, Z.; Yang, N.; Meng, B.: Preparation and oxygen permeation properties of highly asymmetric  $\text{La}_{0.6}\text{Sr}_{0.4}\text{Co}_{0.2}\text{Fe}_{0.8}\text{O}_{3-\alpha}$  perovskite hollow-fiber membranes. *Ind. Eng. Chem. Res.* **48**, 510–516 (2008)
  22. Innocenzi, P.; Malfatti, L.; Costacurta, S.; Kidchob, T.; Piccinini, M.; Marcelli, A.: Evaporation of ethanol and ethanol–water mixtures studied by time-resolved infrared spectroscopy. *J. Phys Chem* **112**, 6512–6516 (2008)
  23. Delbos, C.; Lebain, G.; Richet, N.; Bertail, C.: Performances of tubular  $\text{La}_{0.8}\text{Sr}_{0.2}\text{Fe}_{0.7}\text{Ga}_{0.3}\text{O}_{3-\delta}$  mixed conducting membrane reactor for under pressure methane conversion to syngas. *Catal. Today.* **156**, 146–152 (2010)
  24. Wu, Z.; Wang, B.; Li, K.: Functional LSM-ScSZ/NiO-ScSZ dual-layer hollow fibres for partial oxidation of methane. *Int. J. Hydrogen Energy* **36**, 5334–5341 (2011)
  25. Ahmad, S.H.; Jamil, S.M.; Othman, M.H.D.; Rahman, M.A.; Jaafar, J.; Ismail, A.F.: Co-extruded dual-layer hollow fiber with different electrolyte structure for a high temperature micro-tubular solid oxide fuel cell. *Int. J. Hydrogen Energy* **42**, 9116–9124 (2017)
  26. Iqbal, R.M.; Nurherdiana, S.D.; Hartanto, D.; Othman, M.H.D.; Fansuri, H.: Morphological control of  $\text{La}_{0.7}\text{Sr}_{0.3}\text{Co}_{0.2}\text{Fe}_{0.8}\text{O}_{3-\delta}$  and  $\text{La}_{0.7}\text{Sr}_{0.3}\text{MnO}_{3-\delta}$  catalytic membrane using PEG- $\text{H}_2\text{O}$  additive. *IOP Conf. Ser. Mater. Sci. Eng.* (2018). <https://iopscience.iop.org/article/10.1088/1757-899X/348/1/012008>. Accessed 31 Jan 2019.
  27. Sandoval, M.V.; Matta, A.; Matencio, T.; Domingues, R.Z.; Ludwig, G.A.; De Angelis Korb, M.; De Fraga Malfatti, C.; Gauthier-Maradei, P.; Gauthier, G.H.: Barium-modified NiO-YSZ/NiO-GDC cermet as new anode material for solid oxide fuel cells (SOFC). *Solid State Ionics* **261**, 36–44 (2014)
  28. Tan, X.; Wang, Z.; Liu, H.; Liu, S.: Enhancement of oxygen permeation through  $\text{La}_{0.6}\text{Sr}_{0.4}\text{Co}_{0.2}\text{Fe}_{0.8}\text{O}_{3-\delta}$  hollow fibre membranes by surface modifications. *J. Memb. Sci.* **324**, 128–135 (2008)

